

Article

Modeling of a Pilot-Scale Fixed-Bed Reactor for Dehydration of 2,3-Butanediol to 1,3-Butadiene and Methyl Ethyl Ketone

Daesung Song

Global Technology, SK Innovation, 325 Exporo, Yuseong-gu, Daejeon 305-712, Korea; daesungs@gmail.com;
Tel.: +82-10-9312-6098

Received: 13 January 2018; Accepted: 7 February 2018; Published: 9 February 2018

Abstract: A 1D heterogeneous reactor model accounting for interfacial and intra-particle gradients was developed to simulate the dehydration of 2,3-Butanediol (2,3-BDO) to 1,3-Butadiene (1,3-BD) and Methyl Ethyl Ketone (MEK) over an amorphous calcium phosphate (a-CP) catalyst in a pilot-scale fixed-bed reactor. The developed model was validated with experimental data in terms of a fluid temperature profile along with the length of the catalyst bed, 2,3-BDO conversion, and selectivity for the major products, 1,3-BD and MEK, at the outlet of the reactor. The fluid temperature profile obtained from the model along the length of the catalyst bed coincides satisfactorily with the experimental observations. The difference between the experimental data and the 1D heterogeneous reactor model prediction for 2,3-BDO conversion and selectivity of 1,3-BD and MEK were 0.1%, 9 wt %, and 2 wt %, respectively. In addition, valuable insights related to the feeding system of a commercial-scale plant were made through troubleshooting of the pilot tests. Notably, if the feed including only 2,3-BDO and furnaces that increase the temperature of the feed to the reaction temperature were used in a commercial plant, the feeding system could not be operational because of the presence of heavy chemicals considered oligomers of 2,3-BDO.

Keywords: 2,3-Butanediol dehydration; 1,3-Butadiene; Methyl Ethyl Ketone; amorphous calcium phosphate; reactor modeling; pilot-scale fixed-bed reactor

1. Introduction

1,3-BD and MEK are widely used in various industrial fields. However, these compounds are mainly prepared from petroleum, which is a finite resource and a major cause of regional disparities and environmental pollution. 2,3-BDO has been considered as a potential intermediate for the production of hydrocarbons including 1,3-BD and MEK because 2,3-BDO can be produced through bio-fermentation using various biomasses, synthetic gases (syngas) from coal gasification, and industrial gas waste as feedstock [1–3].

Research on the dehydration of 2,3-BDO to 1,3-BD and MEK using various catalysts has been conducted by several research group since the 1940s. The catalysts are bentonite clay [4], metal and earth oxides [5–9], zeolites [10–13], a perfluorinated resin with sulfonic acid groups [10], heteropolyacids [11,14], calcium phosphates [15–20], Cs/SiO₂ [21], sodium phosphates [22] and so on. Research on old chemistry and new catalytic advances in the on-purpose synthesis of butadiene has been reviewed by Makshina et al. [23]. Duan et al. [24] prospected future of the production of 1,3-butadiene from butanediols. However, most research was conducted to identify dehydration catalysts or reaction conditions that produce good performance. Recently, reaction kinetics and a deactivation model of the dehydration of 2,3-BDO to 1,3-BD and MEK over a-CP catalyst were proposed [18,19]. In addition, a process design for the recovery of 1,3-BD and MEK

from BDO-dehydration products, which were obtained from lab-scale experiments, was proposed as a conceptual design for the industrial scale [25].

Development of reactor model and pilot-scale tests of a reactor are essential for commercialization of the 2,3-BDO dehydration process. However, to our knowledge, research on modeling and pilot-scale tests of a reactor for dehydration of 2,3-BDO to 1,3-BD and MEK has not been done. The purpose of this work is, therefore, to develop a suitable reactor model for the dehydration of 2,3-BDO to 1,3-BD and MEK over a-CP catalyst and to validate the reactor model against experimental data obtained using a pilot-scale fixed-bed reactor.

The pilot-scale fixed-bed reactor was simulated by a one-dimensional (1D) heterogeneous reactor model. The simulation results were compared with the experimental data in terms of fluid temperature profile along with length of catalyst bed, 2,3-BDO conversion, and selectivity for the major products at the outlet of the reactor. In addition, valuable insights related to the feeding system of a commercial-scale plant were made when troubleshooting the pilot tests. The reactor model, experimental data, and investigation are anticipated to be very useful when the 2,3-BDO dehydration process is commercialized.

2. Results and Discussion

The 1D heterogeneous reactor model accounting for interfacial and intra-particle gradients was validated with the test results of the pilot-scale fixed-bed reactor. The simulation results were compared with the experimental data of test 2 in terms of the fluid temperature profile along with the length of the catalyst bed, conversion of 2,3-BDO, and selectivity for the major products at the outlet of the reactor. Average values of operating conditions, temperature in the catalyst bed, and product compositions were used for the comparison.

In Figure 1, the solid line represents the fluid temperature obtained from the reactor model along the length of the catalyst bed, while the scattered points show the measured temperature. As is evident in the figure, the fluid temperature profile coincides satisfactorily with the experimental observations. The fluid temperature decreases rapidly from the inlet of the catalyst bed to the point at 0.05 m because of the endothermic nature of the reactions, the higher temperature, and the greater concentration of reactant, 2,3-BDO, near the inlet of the reactor. The fluid temperature decreases slowly from 0.05 to 0.29 m owing to the reduced temperature and concentration of the reactant. After 0.29 m, the temperature increases because nearly 100% of the reactant is consumed, so there are no reactions taking place and heat transfers from the outside of the reactor to the catalyst bed.

Figure 2 also represents good performance of the model for the prediction of 2,3-BDO conversion and selectivity of the target products, 1,3-BD and MEK, at the outlet of the catalyst bed in spite of the discrepancies between model prediction and experimental result when it comes to the selectivities of the low concentration components 3B2OL and 2-methylpropanal (2MPL). The experimental 1,3-BD selectivity is higher than the simulated one because the experimental selectivity of 3B2OL, which is the intermediate product of 1,3-BD, and 2MPL, which is the other product produced from 2,3-BDO, is less than the simulated one. This result means that the route leading to the formation of 3B2OL and then to the formation 1,3-BD from 3B2OL would be more active than the simulation result expects. In addition to that, impurities are not considered in the reaction products since the total amount of minor butene isomers and heavy compounds made by polymerization of 1,3-BD [19] are less than 0.7 wt % over all experiments. This assumption would lead to the higher experimental selectivity of 1,3-BD and the lower experimental selectivity of 3B2OL and 2MPL.

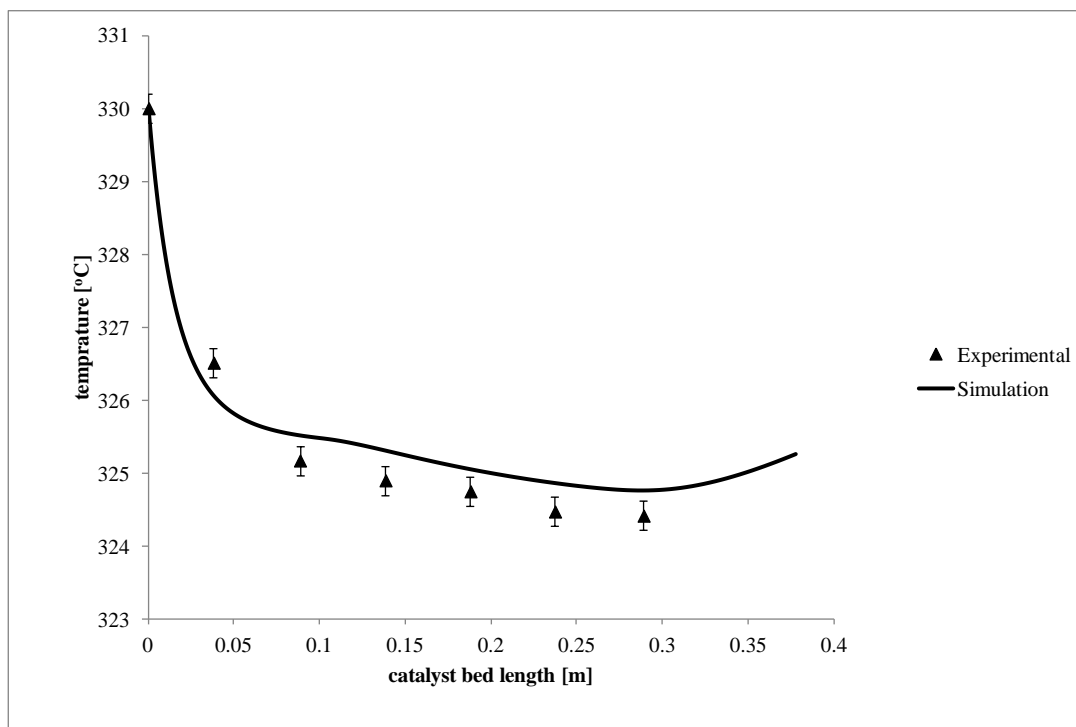


Figure 1. Comparison of the fluid temperature profiles of simulated and experimental data.

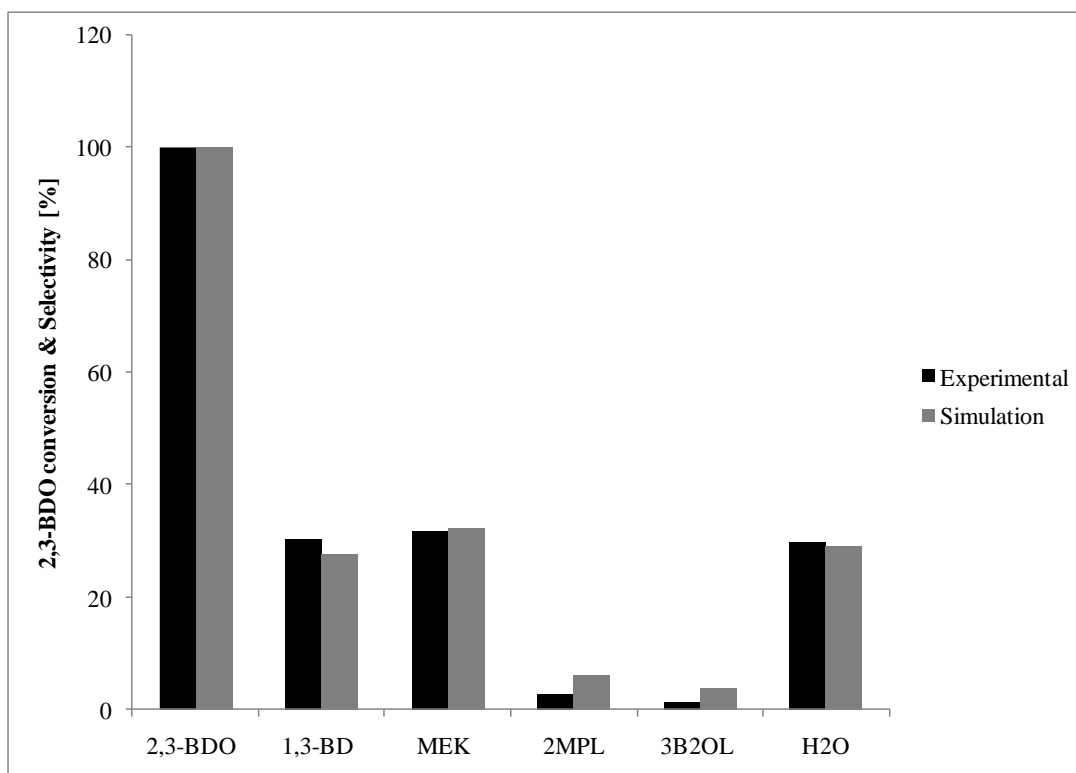


Figure 2. Comparison of 2,3-BDO conversion and selectivity of the major products between the simulated and experimental data.

3. Experimental Studies

3.1. Experimental Setup

Figure 3 illustrates a schematic drawing of the reaction system used for the dehydration of 2,3-BDO. 2,3-BDO including 1.45% water (98.65%, Sigma-Aldrich, St. Louis, MO, USA) was fed to the reactor by an HPLC pump (P1) to a ceramic fiber heater (CFH1) and N₂ as a carrier gas was fed through a line heater (LE1) to raise it to the reaction temperature by a mass flow meter (MFM). 2,3-BDO reached the reaction temperature by passing through three ceramic fiber heaters (CFH1-3). The heated mixture of 2,3-BDO and N₂ was fed to one of two reactors (R1&R2) through a line mixer and the temperature of the reactors was maintained by electric heaters around R1 and R2. The product of the reactor was cooled by a cooler (HE1). The condensed mixture was split into gas and liquid phases through sight glasses (SG1&SG2). A liquid sample was collected from SG1 and SG2. The gas stream from the sight glasses went to the flow transmitter (FT) and a gas sample was collected through the sample point with a gas bag.

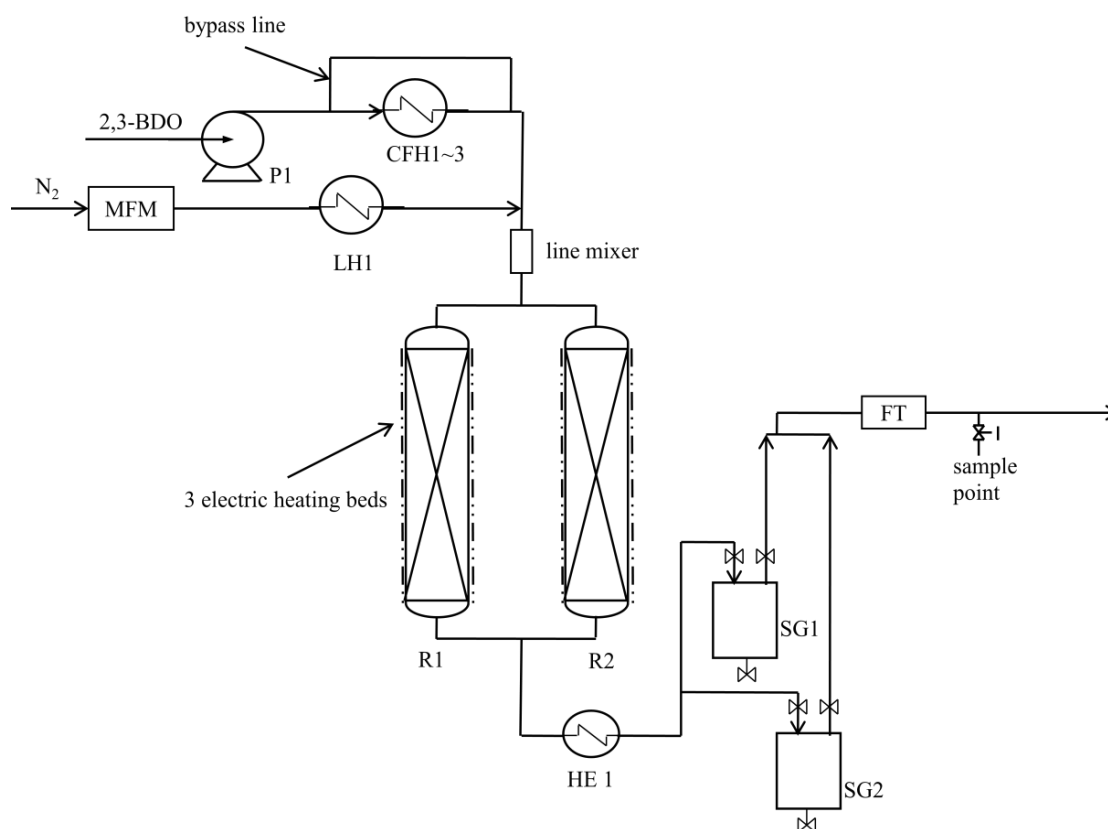


Figure 3. Schematic of the reaction system for the dehydration of 2,3-BDO.

Figure 4 shows a scheme of the fixed-bed reactor. Amorphous calcium phosphate catalysts, prepared by a co-precipitation method as in previous work [18,19], were crushed, sieved through a 16–40 mesh filter, and loaded into a space between 552 mm from the top of the reactor and 256 mm from the bottom. Other parts of the reactor were filled with 3.2 mm spherical silica beads. An additional thermocouple tube was installed at the center of the reactor so that temperature-detecting sensors (T1–T7) could be inserted into the reactor. T1 was located at 414 mm from the top of the reactor. The inlet temperature of the catalyst bed was checked by T1. T2–T7 were located at 38, 88, 138, 188, 238, and 288 mm from the top of the catalyst bed. Temperature profiles inside the catalyst bed were obtained through T2–T7. The detailed reactor specifications are summarized in Table 1.

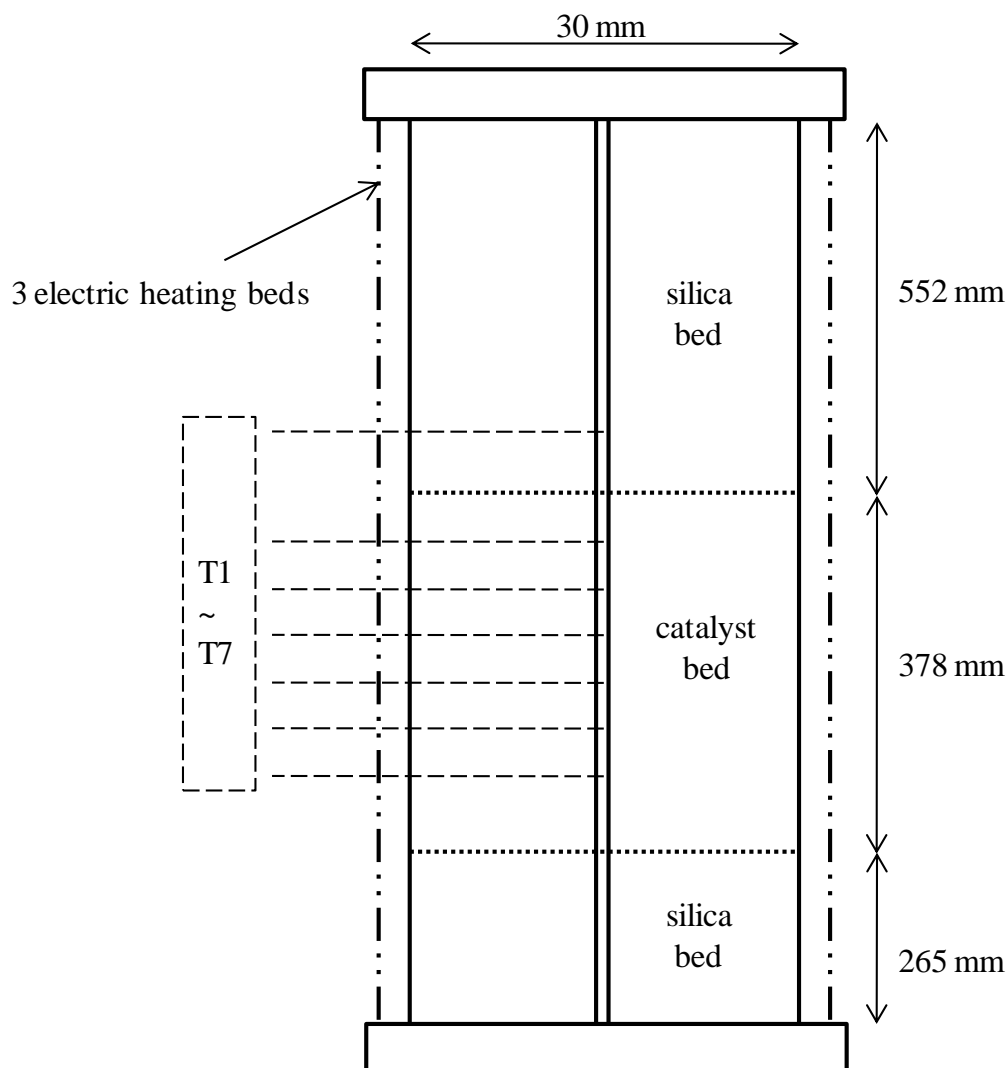


Figure 4. Scheme of the fixed-bed reactor.

Table 1. Reactor specifications.

	Property	Value	Unit
Catalyst	Type	Amorphous Calcium Phosphate (Ca/P = 1.3)	
	average diameter	2.855	mm
	weight	80	g
	density	460.5	kg/m ³
	heat capacity [26]	995	J/(kg K)
	conductivity	0.251	W/(m K)
	porosity	0.121	-
	tortuosity [27,28]	1.73	-
tube	inner diameter	30	mm
	tube length	1195	mm
tube wall	thickness	3.937	mm
	thermal conductivity	16	W/(m K)
	heat capacity	2000	J/(kg K)
catalyst bed	length	378	mm
	density	299.4	kg/m ³
	porosity	0.35	-

3.2. Operation and Troubleshooting

Initially, 800 g/h N₂ was fed into the reaction system for 6 h to purge the system and establish the reaction temperature. Then, the flow rate of N₂ and 2,3-BDO and the temperature of T1 used as the inlet temperature of the catalyst bed were set to the operating conditions shown in Table 2 by MFC, P1, CHF1-3, and LH1 as shown in Figure 3 for 2 h. The wall temperature of the reactor tube was maintained by 3 electric heating beds during the tests. The product stream of the reactor was cooled by HE1. The temperature of HE1 was maintained as 25 to 30 °C to avoid freezing unreacted 2,3-BDO, which freezes at around 20 °C at 1 bar.

During the operation using R1 after the initial work mentioned above for test 1, which was without an N₂ feed, the pressure of P1 was increased sharply because the line passing through CHF1-3 was blocked with heavy chemicals thought to be oligomers of 2,3-BDO. The reasons for formation of the oligomers were most likely a long residence time of 2,3-BDO in CHF1-3 and local hot spots on the line surface generated by CHF1-3. This means that if the feed including only 2,3-BDO and the furnaces to increase the temperature of the feed to the reaction temperature would be used in a commercial plant, the feeding system could not be operational because of the oligomers of 2,3-BDO. Design of a stable 2,3-BDO feeding system would be essential to commercializing the 2,3-BDO dehydration process. To solve the problem in the pilot-scale reaction system, a bypass line as shown in Figure 3 was installed to bypass CHF1-3 and the temperature of T1 was maintained at a constant temperature by electric heat beds around the reactor without using CHF1-3.

Test 2 was performed continuously in the other reactor, R2. After the initial work discussed above, the reactor was operated for 6 h under the operating conditions of test 2 to reach a steady state, which was assessed by the temperature profile of the catalyst bed, and then was operated for 16 h under the same conditions to obtain gas and liquid samples every 4 h. Ideally, tests for different inlet conditions are necessary to validate the model. However, a-CP catalyst in the lab-scale tests under the operating conditions of test 2 was deactivated sharply in 24 h [19]. To remove the deactivation effects, tests for different inlet conditions were not implemented. The data from test 2 were used for a preliminary validation.

Table 2. Reactor operating conditions.

Operating Conditions	Test 1	Test 2	Unit
inlet temperature of the catalyst bed	330	330	°C
pressure	1	1	bar
N ₂ flow rate	0	393	g/h
2,3-BDO flow rate	80	39	g/h
temperature of 3 electric heating beds	330	330	°C

3.3. Analysis Methods

The same analysis methods as were used in previous research [19] were used here. The compositions of the gas and liquid samples were analyzed in a gas chromatograph (GC, Agilent 7890A, Santa Clara, CA, USA) with a DB-1 column (non-polar phase, 60 m × 0.250 mm × 1 μm) and a Flame Ionization Detector (FID) for analysis of the hydrocarbon content. The compositions of major components were normalized to remove the effects of impurities. The conversion of 2,3-BDO and the selectivity for each product were computed as follows:

$$X_{2,3-BDO} = \frac{F_{BDO,in} - F_{BDO,out}}{F_{BDO,in}} \times 100, \quad (1)$$

$$S_n = \frac{F_{n,out}}{F_{total} - F_{BDO,out} - F_{N_2}} \times 100, \quad (2)$$

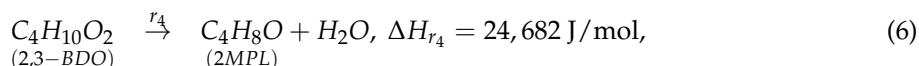
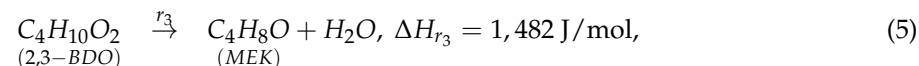
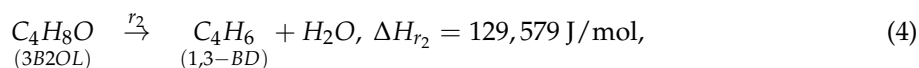
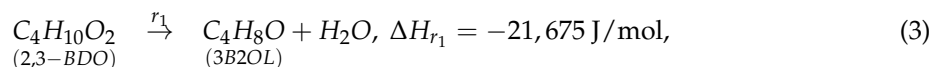
where $X_{2,3-BDO}$ is the conversion of 2,3-BDO, n is a component of the product, S is the mass and F is the mass flow rate.

The composition of water was calculated by the reaction stoichiometry of Equations (3)–(6) in Section 4.1 based on the compositions of 3-Buten-2-ol(3B2OL), 1,3-BD, MEK, and 2-Methylpropanal (2MPL) in the gas and liquid samples.

4. Development of the Reactor Model

4.1. Reaction Kinetics

The reaction kinetics of the dehydration of 2,3-BDO to 1,3-BD and MEK using a-CP as a catalyst, as in previous research [18], were used for the reactor model. The major pathways of 2,3-BDO dehydration are described by the following reactions:



The reaction rates based on the power law are:

$$r_i = k_i C_{\text{react},i}^{n_i}, \quad (7)$$

where

$$C_j = \frac{P_j}{RT}, \quad (8)$$

$$k_i = k_{T_{\text{ref}},i} \exp\left(\frac{-E_i}{R} \left(\frac{1}{T} - \frac{1}{T_{\text{ref}}}\right)\right), \quad (9)$$

where i is the number of reaction, r is the reaction rate, react is the reactant, C is the mole concentration, n is the reaction order, j is the number of species, P is the pressure, R is the ideal gas law constant, T is the temperature in bulk gas phase, k is the reaction rate constant, $k_{T_{\text{ref}}}$ is the transformed adsorption pre-exponential factor, E is the activation energy and T_{ref} is the reference temperature. The kinetic parameter values are shown in Table 3.

Table 3. Kinetic parameters [18].

Model Parameter	Unit	Value
E_1	J/mol	2.33×10^5
E_2	J/mol	2.82×10^5
E_3	J/mol	1.93×10^5
E_4	J/mol	1.66×10^5
$k_{T_{\text{ref}},1}$	$\text{mol}^{(1-n_1)} \text{m}^{3(n_1-1)} \text{s}^{-1}$	7.45×10^{-4}
$k_{T_{\text{ref}},2}$	$\text{mol}^{(1-n_2)} \text{m}^{3(n_2-1)} \text{s}^{-1}$	4.41×10^{-4}
$k_{T_{\text{ref}},3}$	$\text{mol}^{(1-n_3)} \text{m}^{3(n_3-1)} \text{s}^{-1}$	6.44×10^{-4}
$k_{T_{\text{ref}},4}$	$\text{mol}^{(1-n_4)} \text{m}^{3(n_4-1)} \text{s}^{-1}$	1.27×10^{-4}
n_1, n_3, n_4	-	0.0187
n_2	-	0.146

4.2. Reactor Model

The 1D heterogeneous reactor model accounting for interfacial and intra-particle gradients was conducted for reactor modeling. A plug flow was assumed to apply, axial dispersion and thermal conductivity were ignored, and it was assumed that there was no channeling along the reactor tube. Under the above assumptions, the conservation equations are as follows.

For the fluid phase:

$$0 = -\frac{\partial(u_s C_j)}{\partial z} + k_f a_v (C_{ssj} - C_j), \quad (10)$$

$$0 = -\frac{\partial(u_s \rho_f C_p T)}{\partial z} + h_f a_v (T_{ss} - T) - \frac{4}{d_t} U (T - T_w), \quad (11)$$

where z is the axial reactor coordinate, u_s is the superficial fluid velocity, k_f is the mass transfer coefficient between catalyst surface and fluid, a_v is the external particle surface area per unit reactor volume, C_{ss} is the mole concentration at the surface of catalysts, ρ_f is the fluid density, C_p is the fluid heat capacity, h_f is the heat transfer coefficient between catalyst surface and fluid, T_{ss} is the temperature at the surface of catalysts, d_t is the diameter of a reactor, U is the overall heat transfer coefficient and T_w is the temperature of electric heaters around the reactors.

For a cross section of the bed including the solid and fluid phases:

$$k_f a_v (C_{ssj} - C_j) = \rho_B \sum_{i=1}^{rxn} v_{ji} \eta_i r_{si,s}, \quad (12)$$

$$h_f a_v (T_{ss} - T) = \rho_B \sum_{i=1}^{rxn} (-\Delta H_{R_i}) \eta_i r_{si,s}, \quad (13)$$

where ρ_B is the bulk density of catalyst bed, rxn is the number of reactions, v_{ji} is the stoichiometric coefficient of species j in reaction i , η is the effectiveness factor, $r_{si,s}$ is the reaction rate at the surface of the catalyst and ΔH_R is the heat of reaction.

For the solid phase:

$$0 = D_e \left(\frac{\partial^2 C_{sj}}{\partial r_p^2} + \frac{2}{r_p} \frac{\partial C_{sj}}{\partial r_p} \right) + \rho_s \sum_{i=1}^{rxn} v_{ji} r_{si}, \quad (14)$$

$$0 = \lambda_p \left(\frac{\partial^2 T_s}{\partial r_p^2} + \frac{2}{r_p} \frac{\partial T_s}{\partial r_p} \right) + \rho_s \sum_{i=1}^{rxn} (-\Delta H_{R_i}) r_{si}, \quad (15)$$

where D_e is the effective diffusivity within a catalyst, C_s is the mole concentration in catalysts, r_p is the catalyst radius, ρ_s is the catalyst density, r_s is the reaction rate in catalysts, λ_p is the catalyst heat conductivity and T_s is the temperature in catalysts.

Boundary conditions:

$$\begin{aligned} F_j &= F_{j,in}, \quad T = T_{in} \quad \text{at } z = 0 \\ \frac{dC_j}{dr_p} &= 0, \quad \frac{dT}{dr_p} = 0 \quad \text{at } r_p = 0, \quad \forall z \in (0, L_t] \\ C_{sj} &= C_{ss,j}, \quad T_s = T_{ss} \quad \text{at } r_p = d_p/2, \quad \forall z \in (0, L_t] \end{aligned}$$

where F is the mass flow rate, F_{in} is the mass flow rate at the inlet of the catalyst bed, T_{in} is the temperature at the inlet of the catalyst bed, C_{sj} is the mole concentration at the surface of the catalyst, T_s is the temperature at the surface of the catalyst and L_t is the length of catalyst bed.

The pressure drop in the reactor tube was calculated by the classical Ergun equation [29]. Ergun correlations combine the equation for the friction factor in highly turbulent flow in a channel with an equation for laminar flow in an empty conduit. The fluid-to-particle interfacial heat and mass transfer resistance are considered by using Hougen correlation [30], which is based on Colburn j -factor analogy. The correlation relates the j -factor to Reynolds number for packed beds of spheres.

The tube inside heat transfer coefficient is calculated from the effective bed heat conductivity and bed-wall heat transfer coefficient [31]. These two coefficients have both a static and a dynamic contribution, where the static contribution relates to heat transfer in the hypothetical situation of zero flow, and the dynamic contribution accounts for hydrodynamics effects [32]. The relevant correlations and equations for the 1D heterogeneous model are given in Table 4. The methods used to calculate the physicochemical properties of the reactor model are provided in Table 5. The algebraic equations and ordinary differential equations with the boundary conditions of the reactor model were formulated in gPROMS and solved by the numerical DAE solvers named DAEBDF provided by gPROMS [33].

Table 4. Correlations and equations used for the 1D heterogeneous model.

Parameter	Formula
mass and heat transfer coefficient between catalyst surface and fluid [30]	$Sh_p = Re_p Sc^{1/3} \max(1.66 Re_p^{-0.51}, 0.983 Re_p^{-0.41})$ $Nu_p = Re_p Pr^{1/3} \max(1.66 Re_p^{-0.51}, 0.983 Re_p^{-0.41})$
overall heat transfer coefficient [34]	$\frac{1}{U} = \frac{1}{h_i} + \frac{x_w}{\lambda_m} \frac{d_t}{d_L}$
tube inside heat transfer coefficient [31,32]	$\frac{1}{h_i} = \frac{1}{\alpha_{ws}^e} + \frac{(d_i/2) Bi+3}{3\lambda_{rs}^e Bi+4}$ $\alpha_{ws}^e = \alpha_{ws,0}^e + \alpha_{ws,d}^e$ $\lambda_{rs}^e = \lambda_{rs,0}^e + \lambda_{rs,d}^e$
effective diffusivity within a catalyst [35]	$D_e = D_{\text{mean}}(\varepsilon_p/\tau)$
effectiveness factor [35]	$\eta_i = \int_0^{r_p} r_{si} dr / (r_p r_{si,s})$

Table 5. Methods used to calculate physicochemical properties.

Property	Method
fluid density	Peng-Robinson [36]
fluid viscosity	Lucas [36]
fluid heat capacity	ideal gas [36]
fluid conductivity	Steil-Thodos [37]
binary diffusion coefficient, components <i>i</i> and <i>j</i>	Fuller-Schettler-Giddings (FSG) [37]
fluid compressibility factor	Peng-Robinson [36]

5. Conclusions

A 1D heterogeneous reactor model considering interfacial and intra-particle gradients was used to simulate 2,3-BDO dehydration in a pilot-scale fixed-bed reactor. The model was validated with experimental data obtained from the pilot plant in terms of the fluid temperature profile along with the length of the catalyst bed, 2,3-BDO conversion, and selectivity for the major products at the outlet of the reactor. The temperature profile along the length of the catalyst bed coincides satisfactorily with the experimental observations, and the developed model shows good performance for the prediction of 2,3-BDO conversion and selectivity of the target products, 1,3-BD and MEK, at the outlet of the catalyst bed, even though the selectivity of 3B2OL and 2MPL are different. The differences between the experimental data and the 1D heterogeneous reactor model prediction for 2,3-BDO conversion and the selectivity of 1,3-BD and MEK were 0.1%, 9 wt %, and 2 wt %, respectively. On the other hand, the reactor model was validated using preliminary validation data and but needs to be validated with more experimental data for future study.

Valuable insights related to the feeding system of a commercial-scale plant were found through troubleshooting of the pilot tests. If the feed including only 2,3-BDO and furnaces to increase the temperature of the feed to the reaction temperature were used in a commercial plant, the feeding system could not be operated owing to the presence of heavy chemicals that are oligomers of 2,3-BDO.

The design of a stable 2,3-BDO feeding system would be a very important part of the commercialization of the 2,3-BDO dehydration process.

Conflicts of Interest: The author declares no conflict of interest.

Nomenclature

a_v	external particle surface area per unit reactor volume, m^2/m^3
Bi	Biot number, m
C	mole concentration, mol/m^3
C_{pf}	fluid heat capacity, $J/kg\ K$
C_{sj}	mole concentration in catalysts, mol/m^3
$C_{sj,s}$	mole concentration at the surface of the catalyst, mol/m^3
\bar{d}_L	logarithmic mean diameter, m
d_p	diameter of a catalyst, m
d_t	diameter of a reactor, m
D_e	effective diffusivity within a catalyst, m^2/s
D_{mean}	mean diffusivity coefficient, m^2/s
E	activation energy, J/mol
F	mass flow rate, g/s
F_{in}	mass flow rate at the inlet of the catalyst bed, g/s
h_f	heat transfer coefficient between catalyst surface and fluid, $W/m^2\ K$
h_i	tube inside heat transfer coefficient, $W/m^2\ K$
k	reaction rate constant, $mol^{(1-n)}\ m^{3(n-1)}\ s^{-1}$
k_f	mass transfer coefficient between catalyst surface and fluid, m/s
$k_{T_{ref}}$	transformed adsorption pre-exponential factor, m^3/mol
L_t	length of the catalyst bed, m
n	reaction order
Nu_p	Nusselt number for fluid-solid heat transfer
P	pressure, Pa
Pr	Prandtl number for the fluid
r	reaction rate, $mol/kg\text{-cat}\ s$
r_p	catalyst radius, m
r_{si}	reaction rate in catalysts, $mol/kg\text{-cat}\ s$
$r_{si,s}$	reaction rate at the surface of the catalyst, $mol/kg\text{-cat}\ s$
R	ideal gas law constant, $J/mol\ K$
Re_p	Reynolds number for packed bed
S	mass selectivity, %
Sc	Schmidt number
Sh_p	Sherwood number for packed bed
T	temperature, K
T_{in}	temperature at the inlet of the catalyst bed, K
T_s	temperature in catalysts, K
T_{ss}	temperature at the surface of catalysts, K
T_{ref}	reference temperature, K
T_w	temperature of electric heaters around the reactors, K
u_s	superficial fluid velocity, m/s
U	overall heat transfer coefficient, $W/m^2\ K$
X	conversion, %
x_w	tube wall thickness, m
z	axial reactor coordinate, m

Greek Letters

α_{ws}^e	effective bed-wall heat transfer coefficient, W/m ² K
$\alpha_{ws,0}^e$	static term of the effective bed-wall heat transfer coefficient, W/m ² K
$\alpha_{ws,d}^e$	static term of the effective bed-wall heat transfer coefficient, W/m ² K
ΔH_R	heat of reaction, J/mol
ε_p	catalyst porosity
η	effectiveness factor
λ_m	wall thermal conductivity, W/m K
λ_p	catalyst heat conductivity, W/m K
λ_{rs}^e	effective bed heat conductivity, W/m K
$\lambda_{rs,0}^e$	static term of effective bed heat, W/m K
$\lambda_{rs,d}^e$	dynamic term of effective bed heat conductivity, W/m K
ν_{ji}	stoichiometric coefficient of species j in reaction i
ρ_B	bulk density of catalyst bed, kg/m ³
ρ_f	fluid density, kg/m ³
ρ_s	catalyst density, kg/m ³
τ	catalyst tortuosity

Subscripts

i	reaction i
j	species j
react	reactant
rxn	reaction

References

- Daniell, J.; Köpke, M.; Simpson, S.D. Commercial biomass syngas fermentation. *Energies* **2012**, *5*, 5372–5417. [[CrossRef](#)]
- Kopke, M.; Mihalcea, C.; Liew, F.; Tizard, J.H.; Ali, M.S.; Conolly, J.J.; Al-Sinawi, B.; Simpson, S.D. 2,3-Butanediol Production by Acetogenic Bacteria, an Alternative Route to Chemical Synthesis, Using Industrial Waste Gas. *Appl. Environ. Microbiol.* **2011**, *77*, 5467–5475. [[CrossRef](#)] [[PubMed](#)]
- Zheng, Q.; Wales, M.D.; Heidlage, M.G.; Rezac, M.; Wang, H.; Bossmann, S.H.; Hohn, K.L. Conversion of 2,3-butanediol to butenes over bifunctional catalysts in a single reactor. *J. Catal.* **2015**, *330*, 222–237. [[CrossRef](#)]
- Bourns, A.N.; Nicholls, R.V.V. The Catalytic Action of Aluminium Silicates: I. The Dehydration of Butanediol-2,3 and Butanone-2 over Activated Morden Bentonite. *Can. J. Res.* **1947**, *25b*, 80–89. [[CrossRef](#)]
- Winfield, M.E. The catalytic dehydration of 2,3-butanediol to butadiene. *Aust. J. Sci. Res. Ser. A* **1945**, *3*, 290–305.
- Winfield, M.E. The Catalytic Dehydration of 2,3-Butanediol to Butadiene. II. Adsorption Equilibria. *Aust. J. Sci. Res. Ser. A* **1950**, *3*, 290–305.
- Kannan, S.V.; Pillai, C.N. Dehydration of meso- and dl-hydrobenzoins and 2,3-butanediols over alumina. *Indian J. Chem.* **1969**, *7*, 1164–1166.
- Duan, H.; Sun, D.; Yamada, Y.; Sato, S. Dehydration of 2,3-butanediol into 3-buten-2-ol catalyzed by ZrO₂. *Catal. Commun.* **2014**, *48*, 1–4. [[CrossRef](#)]
- Duan, H.; Yamada, Y.; Sato, S. Applied Catalysis A: General Efficient production of 1,3-butadiene in the catalytic dehydration of 2,3-butanediol. *Appl. Catal. A Gen.* **2015**, *491*, 163–169. [[CrossRef](#)]
- Bucsi, I.; Molnár, Á.; Bartók, M.; Olah, G.A. Transformation of 1,3-, 1,4- and 1,5-diols over perfluorinated resinsulfonic acids (Nafion-H). *Tetrahedron* **1995**, *51*, 3319–3326. [[CrossRef](#)]
- Molnár, Á.; Bucsi, I.; Bartók, M. Pinacol rearrangement on zeolites. *Stud. Surf. Sci. Catal.* **1988**, *41*, 203–210. [[CrossRef](#)]

12. Lee, J.; Grutzner, J.B.; Walters, W.E.; Delgass, W.N. The conversion of 2,3-butanediol to methyl ethyl ketone over zeolites. *Stud. Surf. Sci. Catal.* **2000**, *130*, 2603–2608. [[CrossRef](#)]
13. Zhang, W.; Yu, D.; Ji, X.; Huang, H. Efficient dehydration of bio-based 2,3-butanediol to butanone over boric acid modified HZSM-5 zeolites. *Green Chem.* **2012**, *14*, 3441–3450. [[CrossRef](#)]
14. Tsrsk, B.; Bucsi, I.; Beregsz, T.; Kapocsi, I.; Molnir, A. Transformation of diols in the presence of heteropoly acids under homogeneous and heterogeneous conditions. *J. Mol. Catal. A Chem.* **1996**, *107*, 305–311.
15. Hahn, H.-D.; Dämbkes, G.; Rupprich, N.; Bahl, H.; Frey, G.D. Butanols. *Ullmanns Encycl. Ind. Chem.* **2013**, 1–13. [[CrossRef](#)]
16. Kim, S.J.; Seo, S.O.; Park, Y.C.; Jin, Y.S.; Seo, J.H. Production of 2,3-butanediol from xylose by engineered *Saccharomyces cerevisiae*. *J. Biotechnol.* **2014**, *192*, 376–382. [[CrossRef](#)] [[PubMed](#)]
17. Nikitina, M.A.; Sushkevich, V.L.; Ivanova, I.I. Dehydration of 2,3-butanediol over zeolite catalysts. *Pet. Chem.* **2016**, *56*, 230–236. [[CrossRef](#)]
18. Song, D. Kinetic Model Development for Dehydration of 2,3-Butanediol to 1,3-Butadiene and Methyl Ethyl Ketone over an Amorphous Calcium Phosphate Catalyst. *Ind. Eng. Chem. Res.* **2016**, *55*, 11664–11671. [[CrossRef](#)]
19. Song, D. Development of a deactivation model for the dehydration of 2,3-butanediol to 1,3-butadiene and methyl ethyl ketone over an amorphous calcium phosphate catalyst. *Ind. Eng. Chem. Res.* **2017**, *56*, 11013–11020. [[CrossRef](#)]
20. Tsukamoto, D.; Sakami, S.; Ito, M.; Yamada, K.; Ito, M.; Yonehara, T. Production of Bio-based 1,3-Butadiene by Highly Selective Dehydration of 2,3-Butanediol over SiO₂-supported Cesium Dihydrogen Phosphate Catalyst. *Chem. Lett.* **2016**, *45*, 831–833. [[CrossRef](#)]
21. Kim, T.Y.; Baek, J.; Song, C.K.; Yun, Y.S.; Park, D.S.; Kim, W.; Han, J.W.; Yi, J. Gas-phase dehydration of vicinal diols to epoxides: Dehydrative epoxidation over a Cs/SiO₂ catalyst. *J. Catal.* **2015**, *323*, 85–99. [[CrossRef](#)]
22. Kim, W.; Shin, W.; Lee, K.J.; Song, H.; Kim, H.S.; Seung, D.; Filimonov, I.N. Applied Catalysis A: General 2,3-Butanediol dehydration catalyzed by silica-supported sodium phosphates. *Appl. Catal. A Gen.* **2016**, *511*, 156–167. [[CrossRef](#)]
23. Makshina, E.V.; Dusselier, M.; Janssens, W.; Degreève, J.; Jacobs, P.A.; Sels, B.F. Review of old chemistry and new catalytic advances in the on-purpose synthesis of butadiene. *Chem. Soc. Rev.* **2014**, *43*, 7917–7953. [[CrossRef](#)] [[PubMed](#)]
24. Duan, H.; Yamada, Y.; Sato, S. Future prospect of the production of 1,3-butadiene from butanediols. *Chem. Lett.* **2016**, *45*, 1036–1047. [[CrossRef](#)]
25. Song, D.; Yoon, Y.-G.; Lee, C.-J. Conceptual design for the recovery of 1,3-Butadiene and methyl ethyl ketone via a 2,3-Butanediol-dehydration process. *Chem. Eng. Res. Des.* **2017**, *123*, 268–276. [[CrossRef](#)]
26. Kelley, K.K. [Part] 13. *High-Temperature Heat-Content, Heat-Capacity, and Entropy Data for the Elements and Inorganic Compounds*; Bureau of Mines: Washington, DC, USA, 1960.
27. Bhatia, S.K. Directional autocorrelation and the diffusional tortuosity of capillary porous media. *J. Catal.* **1985**, *93*, 192–196. [[CrossRef](#)]
28. Dykhuizen, R.C.; Casey, W.H. An analysis of solute diffusion in rocks. *Geochim. Cosmochim. Acta* **1989**, *53*, 2797–2805. [[CrossRef](#)]
29. Ergun, S. Fluid Flow through Packed Columns. *Chem. Eng. Prog.* **1952**, *48*, 89–94.
30. Hougen, O. Engineering Aspects of Solid Catalysts. *Ind. Eng. Chem.* **1961**, *53*, 509–528. [[CrossRef](#)]
31. Dixon, A.G. An improved equation for the overall heat transfer coefficient in packed beds. *Chem. Eng. Process. Process Intensif.* **1996**, *35*, 323–331. [[CrossRef](#)]
32. Specchia, V.; Baldi, G.; Sicardi, S. Heat Transfer in Packed Bed Reactors with One Phase Flow. *Chem. Eng. Commun.* **1980**, *4*, 361–380. [[CrossRef](#)]
33. Process Systems Enterprise Ltd. *gPROMS Advanced User Guide*; Process Systems Enterprise Ltd.: London, UK, 2004.
34. McCabe, W.L.; Smith, J.; Harriott, P. *Unit Operations of Chemical Engineering*, 6th ed.; McGraw Hill: New York, NY, USA, 2001.
35. Riggs, J.M. *Introduction to Numerical Methods for Chemical Engineer*, 2nd ed.; Texas Tech University Press: Lubbock, TX, USA, 1994.

36. Poling, B.E.; Prausnitz, J.M.; O's Connell, J.P. *The Properties of Gases & Liquids*; McGraw Hill: New York, NY, USA, 2001.
37. Perry, R.H.; Green, D.W. *Perry's Chemical Engineering Hand-Book*; McGraw Hill: New York, NY, USA, 1997.



© 2018 by the author. Licensee MDPI, Basel, Switzerland. This article is an open access article distributed under the terms and conditions of the Creative Commons Attribution (CC BY) license (<http://creativecommons.org/licenses/by/4.0/>).